Article

Multiple Use SiPM Integrated Circuit (MUSIC) for Large Area and High Performance Sensors

Sergio Gómez [1,*,†] **, David Sánchez** [2,†] **, Joan Mauricio** [2] **, Eduardo Picatoste** [2] **, Andreu Sanuy** [2] **, Anand Sanmukh** [2] **, Marc Ribó** [2] **and David Gascón** [2]

1   Institut d'Estudis Espacials de Catalunya (IEEC), University of Barcelona (ICCUB), 08028 Barcelona, Spain
2   Department Física Quàntica i Astrofísica, Institut de Ciències Del Cosmos (ICCUB),
    University of Barcelona (IEEC-UB), 08028 Barcelona, Spain; dsanchez@fqa.ub.edu (D.S.);
    jmauricio@fqa.ub.edu (J.M.); epicatoste@fqa.ub.edu (E.P.); asanuy@fqa.ub.edu (A.S.);
    asanmukh@fqa.ub.edu (A.S.); mribo@fqa.ub.edu (M.R.); dgascon@fqa.ub.edu (D.G.)
*   Correspondence: sgomez@fqa.ub.edu
†   These authors contributed equally to this work.

Abstract: The 8-channel Multiple Use Silicon Photo-multiplier (SiPM) Integrated Circuit (MUSIC) Application specific integrated circuit (ASIC) for SiPM anode readout has been designed for applications where large photo-detection areas are required. MUSIC offers three main features: (1) Sum of the eight input channels using a differential output driver, (2) eight individual single ended (SE) analog outputs, and (3) eight individual SE binary outputs using a time over threshold technique. Each functionality, summation and individual readout includes a selectable dual-gain configuration. Moreover, the signal sum implements a dual-gain output providing a 15-bit dynamic range. The circuit contains a tunable pole zero cancellation of the SiPM recovery time constant to deal with most of the available SiPM devices in the market. Experimental tests show how MUSIC can linearly sum signals from different SiPMs and distinguish even a few photons. Additionally, it provides a single photon output pulse width at half maximum (FWHM) between 5–10 ns for the analog output and a single-photon time resolution (SPTR) around 118 ps sigma using a Hamamatsu SiPM S13360-3075CS for the binary output. Lastly, the summation mode has a power consumption of ≈200 mW, whereas the individual readout consumes ≈30 mW/ch.

Keywords: large detection area; fast front-end electronics; summation; SiPM; scintillators; Cherenkov radiation

1. Introduction

1.1. Applications of Radiation Detectors

The detection of low intensity light radiation with large efficiency and robust detectors is highly in demand for several applications [1]. Many radiation detectors in particle physics experiments, astrophysics, medical imaging and other fields use photo-sensors for large detection areas up to 1 inch or more [2–5]. Two applications of photo-sensors for the detection of elementary particles are the scintillation detectors [6] and the Cherenkov radiation detectors [7]. Scintillators have been extensively used in calorimeters, and also recently in trackers based on scintillating fibres [8,9]. Time-of-flight measurement often requires scintillator detectors as well [10,11]. A classical example of a Cherenkov detector is the Ring Imaging Cherenkov (RICH) used for particle identification [12,13]. Another example is ground-based Cherenkov telescopes that are employed for high-energy gamma-ray stereoscopic observations [14,15]. These telescopes focus the flashes of Cherenkov light with nanosecond duration onto fast photo-sensor arrays where the signal is read-out [16]. Medical imaging, including technologies such as positron emission tomography (PET) [17,18] and gamma single photon emission computed tomography (SPECT), also demand efficient photo-detectors [19,20].

Photo-sensor requirements are different according to the specific detector. Usually, RICH detectors require blue and Ultra-Violet (UV) sensitivity and single photon detection [12]. In contrast, scintillator light yield is much higher and the emission is shifted to the blue/green region of the spectrum [10]. Calorimeters have large dynamic range, up to hundreds or thousands of photons [3], whereas scintillating fiber trackers are used for Minimum Ionizing Particle (MIP) signals, producing few photons [8,21]. Lastly, Imaging Atmospheric Cherenkov Telescopes (IACTs) require a detectable dynamic range from the single photo-electron signal for calibration purposes and up to several thousand photons (5000 PE) for the highest Cherenkov light flashes [4,15,22].

For a long time, the main photo-detectors for such detection systems were the photo-multiplier tubes (PMTs), which were created more than 50 years ago [23]. PMTs are used to convert the detected light into an electrical signal that can be processed by specific readout electronics. In the last decade, a new type of photo-detector, the Silicon Photo-multiplier (SiPM), was developed on the basis of the semiconductor technology as an alternative to PMTs [2,24]. Application specific integrated circuits (ASICs) for radiation sensors, in particular Front End (FE) electronics for SiPMs that are stable and perform at high count rates, are also needed to achieve the best performance from photo-sensor devices [19]. Typically, the FE electronics have to deal with the high terminal capacitance of the SiPMs when large photo-detection areas are required and therefore dedicated ASICs are needed [25].

1.2. SiPM Technology

An SiPM [1,24,26–30] (also known as a Geiger-mode avalanche photo-diode, G-APD) is a device obtained by connecting in parallel several miniaturized Single Photon Avalanche Diode (few tens of μm^2 and referred hereafter as SPAD) [31], belonging to the same silicon substrate. The small SPADs and a quenching element are named micro-cells in the SiPM. The output signal of the SiPM is proportional to the number of SPAD cells that the incident photons activate. Since the over-voltage (i.e., the difference between bias and breakdown voltage) and cell capacitance uniformity can be quite accurate in modern production processes, an excellent separation between peaks in the charge spectrum is achieved [29]. This makes it possible to count even tens of photons, which is clearly impossible with PMTs [23]. PMTs still have some advantages—lower temperature dependence and lower dark count rate [23]. Nevertheless, temperature dependence of the SiPM is related to the breakdown voltage and therefore it can be corrected by smart supply voltage control and temperature stabilization [25].

SiPMs are the main sensors that are a substitute for PMTs in several research fields [6,25,32–35]. These devices are characterized by extremely good timing response, moderate operating bias voltages (lower than 100 V), high gain (equal or larger than PMTs), low-amplitude after-pulses and high quantum efficiency. SiPMs also have the benefit of large flexibility in the creation of 2D arrays of sensors, robustness, compactness, better suited for mass production and insensitivity to magnetic fields. However, SiPM capacitance can be at the level of 15 nF per square inch, which imposes serious requirements for a low noise and high speed readout [19]. A common approach to deal with this problem is to add the signal of several SiPMs [36]. Even in this scenario, requirements are stringent for an ASIC implementation if low noise, high bandwidth and large dynamic range have to be achieved [19].

SiPMs suffer from three main noise sources—dark counts, after-pulsing and cross-talk [1,25,28,29,37]. The noise in SiPM devices is mainly due to the dark count rate—an e/h pair can be thermally generated, triggering an avalanche in a micro-cell without an optical photon impinging on it. The dark noise rate depends on the working temperature and the over-voltage, and is directly proportional to the active area of the device. Other noise sources are correlated to other primary events triggered in one cell. Trapping of the carriers and their delayed release in the avalanche region can cause a second avalanche in the junction, named after-pulse [1]. Trapped carriers can have a lifetime from tens to

hundreds of nanoseconds and the second avalanche can be triggered also after the complete micro-cell recharge, increasing artificially the number of counted events. Optical photons can be produced during the avalanche in a micro-cell introducing an additional noise component. These interactions in adjacent micro-cells of the SiPM may generate optical cross-talk noise. The effect of cross-talk can be reduced with trenches (grooves surrounding each micro-cell), which can have metal-coated sidewalls [26].

SiPM technology has greatly evolved during the last 10 years and can be considered as mature enough, although room for improvement still exists. Current SiPM technologies guarantee a dark count rate of about 100 kHz/mm^2 at room temperature [38]. An optimal device would work with a large Photo Detector Efficiency (PDE) of around 50%, while having a cross-talk typically smaller than 10–20%. Currently, Hamamatsu or FBK devices achieve these performances [29,38–40]. A trade-off exists between PDE and cross-talk, since fill factor and over-voltage should be optimized in opposite directions.

1.3. Front End Electronics

Dedicated multi-channel electronics that are stable and perform at high count-rates are required to fully exploit the advantages of SiPMs [41]. In general, these analog electronics need to perform different tasks such as amplification or filtering with a relatively low power consumption depending on the system requirements. As a guideline, FE electronics or ASICs coupled to SiPMs covering large detection areas (SiPM capacitance ranges from 30 pF to more than 2 nF) should be designed considering the following requirements.

- Current sensing with low input impedance. A current-mode input stage is preferable compared to a voltage-mode approach to sustain high event rates in high speed applications and obtain a fast response to optimize the time performance [42]. A low input impedance is desired in a current-mode implementation to maximize the peak current and thus improve the slew rate of the input signal [25,43].
- Shaping of the input signal. SiPM pulses typically have a long time constant associated with the recharge of the micro-cells. This may cause saturation or distortion because of pile up of pulses and thus causing baseline shifts [29]. This effect results in a reduction of the maximum event rate that an ASIC can handle without degradation. Pole-zero cancellation filters are used to shape the SiPM response [41].
- Pre-amplification to optimize the Signal to Noise Ratio (SNR). The input signal from the SiPM must be amplified to maximize the dynamic range and time performance [41]. Noise must be minimized while at the same time preserving the signal amplitude in order to optimize the SNR [19]. Note that, even if nominal gain of the SiPM is in the order of 10^6, only a fraction of the charge is used after applying a shaper to perform a tail cancellation.
- Multi-channel. The ASIC must be capable of handling the input response of several detectors [2,44–46].
- Combination (summation) of the signal of several SiPMs. Large detection areas have to be covered in some applications. Since the largest SiPM detection area is about 6 × 6 mm^2, smaller than the largest PMT, a solution when a large detection area is required is to add the signal of several SiPMs inside the ASIC [19,30]. Direct parallel connection of several SiPM devices has some drawbacks: extremely large capacitance (introducing limitations in speed and SNR) and difficult equalization of SiPM non-uniformities by over-voltage equalization. A dedicated ASIC adding the signals of several SiPMs covering the same area alleviate this drawback.
- Over-voltage equalization. The breakdown voltage of SiPMs suffers from process variability, although fabrication techniques have improved significantly. The different breakdown voltage of each SiPM is translated in gain non-uniformities when several of them are biased with the same power supply. This is particularly problematic when SiPM signals have to be added. Therefore, FE electronics should allow a DC adjustment of the input voltage connected to the anode or cathode of the SiPM (over-voltage equalization) [44,47].

Several ASICs can be found in the literature suitable for the readout of SiPMs [2,25,44–52]. These ASICs consider some of the previous considerations. For instance, the PreAmplifier for CTA (PACTA) ASIC [49] is a single channel wide-band current-mode FE with 16 bits dynamic range designed in AMS 0.35 μm SiGe technology. It provides a differential output with two different gains and the power consumption is about 100 mW.

An 8-channel ASIC, referred to as NINO [50,51], consists of a current-mode FE with a differential input that provides a non-linear Time-over-Threshold (ToT) response of the SiPM. NINO is designed in IBM 0.25 μm technology and presents a power consumption of 27 mW/ch. These electronics can be employed for time measurements and yield a 64 ps sigma for single-photon time resolution (SPTR) with a Hamamatsu SiPM S13360-3050CS.

An alternative ASIC is the 32-channel Citiroc [44] designed in AMS 0.35 μm SiGe technology and developed by Weeroc [52]. This voltage-mode FE provides an analog response of the SIPM suitable for charge measurements and also provides a trigger signal with a high resolution timing (60–70 ps RMS jitter). This ASIC provides 32 binary trigger outputs (time response), 2 multiplexed charge outputs with two different gains and two ASIC trigger outputs, each one obtained as the OR of the charge and time measurements, respectively. The dual-gain charge measurement contains a shaper, a track and hold or peak detector circuit and an analog buffer. An adjustment of the SiPM bias voltage at the input of the ASIC is possible. The power consumption of the ASIC is 6.26 mW/ch when all stages are activated.

1.4. Overview

This paper presents an 8-channel Multiple Use SiPM Integrated Circuit (MUSIC) [53] ASIC for SiPM anode readout, which implements all the aforementioned functionalities, and is organized as follows. Section 2 details the main blocks of the MUSIC ASIC architecture and its main functionalities, while the experimental setups used are described in Section 3. A detailed performance analysis of the MUSIC ASIC is provided in Section 4. Different applications where the MUSIC ASIC have been employed are discussed in Section 5 and some conclusions are drawn in Section 6.

2. Materials: MUSIC Architecture

This section details the main features of the MUSIC chip architecture. Firstly, a description of the different functionalities of the chip are outlined. Secondly, the main aspects of the input stage based on a current preamplifier and the pole zero cancellation circuit to cope with several time constants are described. Thirdly, the summation circuit proposed to add the incoming signals from the different channels and the individual readout are presented. Lastly, a summary of the main characteristics of the ASIC is provided.

2.1. Functional Modes

MUSIC provides several functionalities using multiple copies of the input current readout from each SiPM. Figure 1 illustrates the architecture of the ASIC. The different operational modes are described next.

- Summation: The sum of the input signals is provided as a dual-gain output in differential mode using a high gain and a low gain current from the input readout circuit. The 8 channels contributing to the sum can be controlled individually.
- Individual analog readout: The SiPM response is provided as a single ended analog output per channel in voltage mode.
- Individual binary discriminated output: A non-linear Time-over-Threshold (ToT) response with a pulse width proportional to the input peak current (charge) is generated per channel. Each binary output is provided in single ended mode.
- Fast OR trigger: A trigger signal is provided by performing a logic OR operation between all discriminated channels. The rising edge of this signal indicates whether a valid event has occurred or not. For instance, a signal above dark count noise.
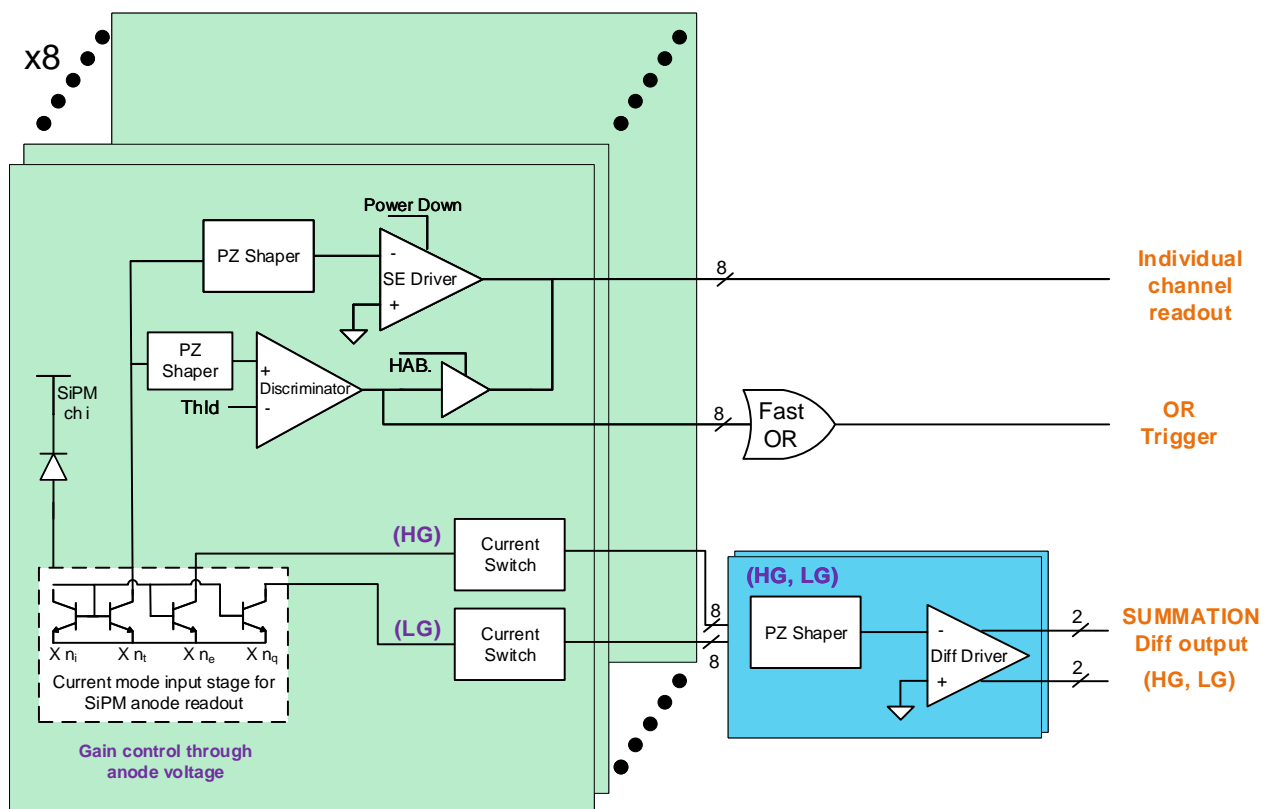
Figure 1. Multiple Use Silicon Photo−multiplier (SiPM) Integrated Circuit (MUSIC) functional block diagram. *HG* refers to high gain and *LG* to low gain signal paths.

For each individual channel, only the analog or digital output can be selected since both signals share the same output pad. Moreover, a selectable dual-gain configuration is available for each functionality, the channel sum and the 8 individual outputs. All these functionalities allow the possibility to apply a Pole-Zero cancellation. Other blocks are included to set the correct operating points of the circuit and configure several tunable parameters. It is important to highlight that every block and channel can be disabled (power down mode) with a specific control signal. Lastly, all these parameters can be reconfigured using an SPI (Serial Parallel Interface) protocol and an external Field-programmable gate array (FPGA) or micro-controller.

2.2. Input Current Stage

An input stage based on a bipolar current mirror with double feedback loop is employed for SiPM anode readout [54]. The aim of this readout circuit is to provide a low input impedance in order to avoid affecting the timing behavior of the SiPM and increase input current. A schematic view of the input stage is illustrated in Figure 2.

The input part of the FE electronics works as follows. The Low Frequency Feedback loop (LF_{FB}) (based on [55]) controls the DC voltage (Va_{ref}) of the input node through the virtual short circuit of a folded cascode operational transconductance amplifier (OTA_1) [56]. This OTA_1 drives a follower closing the LF_{FB} loop. The High Frequency feedback path (HF_{FB}) employs a common-gate regulated cascode configuration [57] in order to keep the input impedance constant over the bandwidth of interest and thus the fast timing behavior of the SiPM is not affected. The design has been implemented taking into account that the dominant pole should be set at the input node (SiPM parasitic capacitance is in the order of tenths of pF). In this way, stability is not compromised when an important capacitance is added at the input.
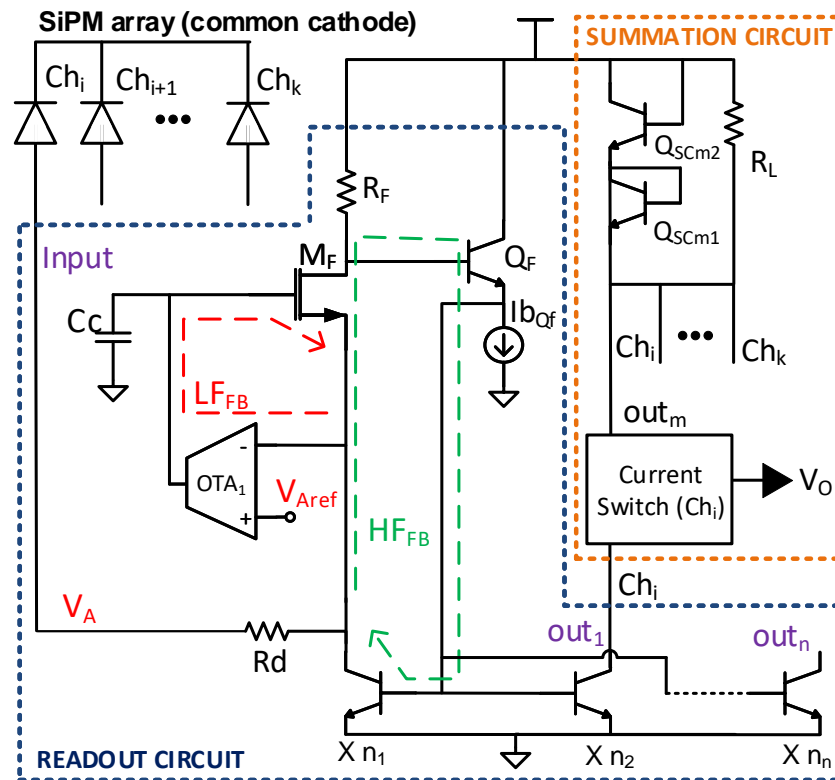
Figure 2. Input current stage including the readout circuit and the summation block.

The current division scheme splits the input current into differently scaled copies. These signals are connected to independent current mirrors to implement the different features described in Section 2.1. The main characteristics of the input stage block are detailed next.

- Low input impedance of ≈32 Ω in the bandwidth of interest.
- Anode connection for multi-channel common cathode SiPM arrays.
- Control of the SiPM bias voltage per channel by individual adjustment of the anode voltage (V_{Aref}). It is configured using an internal 9-bit DAC with 1 V full scale. This adjustment may be used to change the gain or the photon detection efficiency (PDE) of the SiPM, and thus equalize the gain in each channel.
- Large Gain Bandwidth (GBW) of more than 500 MHz.
- Low input referred noise for sensor capacitances between 10 pF to 10 nF: (1) series noise lower than 2 nV/sqrt(Hz); (2) parallel noise lower than 20 pA/sqrt(Hz).
- Low power consumption of about 5 mW/ch.
- Power down mode for each individual channel.

2.3. Pole-Zero Cancellation (PZ Shaper)

The circuit contains a configurable Pole-Zero cancellation (PZ) of the SiPM recovery time constant to deal with sensors from different manufacturers. The PZ reduces the peak duration of the signal and the tail produced by the sensor, but also attenuates the peak amplitude. The equation that defines the behavior of the shaper can be obtained using the schematic view depicted in Figure 3a. The output signal after the PZ compensation (V_O) is defined as follows

$$V_O = \left(\frac{R_2}{R_1 + R_2} \right) \frac{R_1 C_1 s + 1}{R_1 || R_2 C_1 s + 1} V_i. \tag{1}$$

Thus, the time constant can be computed as:

$$\tau = R_1 C_1. \tag{2}$$

The resistors (R_1 and R_2) can be configured with 8 different options (3 bits) and the capacitor (C_1) has 32 possibilities (5 bits). The PZ shaper must be carefully tuned in order to: (1) Cancel the time constant related to the SiPM long tail; (2) compensate the undershoot/overshoot of the signal; (3) minimize the spill over or increase data rate (two events can be overlapped due to the slow tails) by reducing the Full Width at Half Maximum (FWHM) of the output signal and; (4) not jeopardize the signal peak due to excessive attenuation. For instance, increasing pull-up resistor (R_2) will reduce current removed from the input and thus decrease signal attenuation. A good matching with the input time constant will provide a flat output. Figure 3b shows a normalized typical signal before and after PZ compensation.

Decay times up to 100 ns are supported, covering most of the available SiPM devices in the market. The PZ cancellation provides output signals with a FWHM up to 5 ns to 10 ns depending on the SiPM and can be used or bypassed in any operation mode. This 5–10 ns FWHM enables a data rate up to 100 Mcps. In conclusion, there exists a trade-off between the peak amplitude (or SNR) and the FWHM resolution and thus the optimal PZ configuration depends on the requirements of each application.
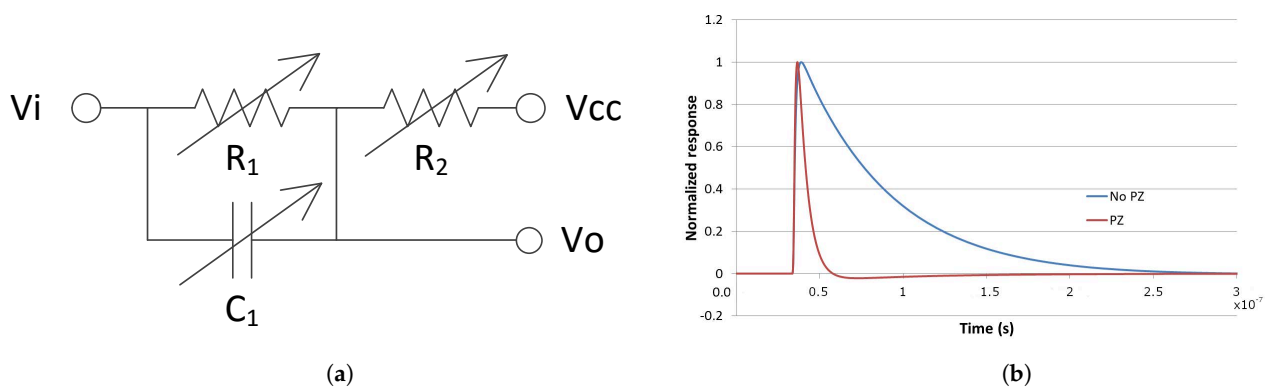

(**a**)　　　　　　　　　　　　　　　　　　　　　　　　　　　　(**b**)

Figure 3. Pole−Zero (PZ) compensation. (**a**) PZ shaper circuit with tunable R_1, R_2 and C_1. (**b**) Normalized response of a single photon using a Hamamatsu SiPM S13350−6050CS with and without PZ cancellation. In this example, the peak signal after the PZ shaper was attenuated an $\approx$35%.

2.4. Summation Circuit

An analog transistor FE was developed to sum, shape and amplify the SiPM signals of one pixel to a composite output without the drawback of summing the sensors capacitance. The summation circuit for adding one or more signals received from a SiPM array is under patent [54]. The input signals can be added by simply connecting the output currents dedicated to summation from each input readout circuit, as previously described in Figure 2. However, if a single photo-diode is not functioning properly or gain non-uniformity exist between inputs, the result may be erroneous. The channel summing module allows conditioned addition of one or more signals provided by the readout circuit in order to solve this problem.

In operation mode, each photoelectric pixel may be sensed by the corresponding readout circuit and then summed at the current switch (CS), as detailed in Figure 2. The current switch implementation is depicted in Figure 4. It acts as an active cascode for the input current mirror and consists of two common base transistors $Q_{CBm,n}$ and a classic two stage Miller Operational Transconductance Amplifier (OTA$_2$) [58]. The active cascode element sets the collector voltage of each slave mirror to the same collector voltage (V_A) of the input transistor. This minimizes channel modulation errors (non-linearity). The $Q_{CBm,n}$ transistor connected to the output of OTA$_2$ works as a current buffer of the input current.
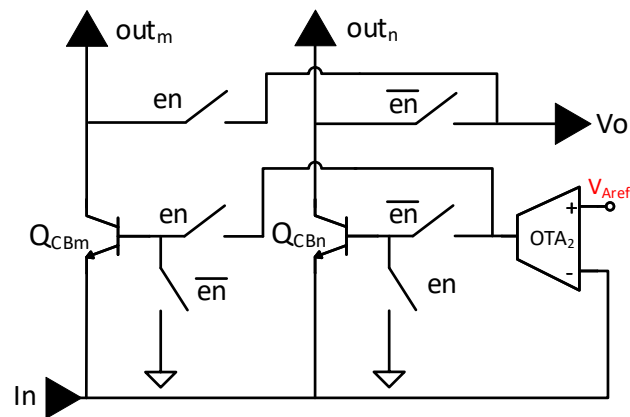
Figure 4. Implementation of the summing current switch. out_m is used for the high gain output and out_n for the low gain.

The summation element CS permits to disconnect one or more channels from the summing module. Note that each readout channel is coupled to a different current switch and then each output out_m of each CS is connected together to sum the different channels (analogously for output out_n). Each output of the summing element has a saturation control (transistors $Q_{SCm_{1,2}}$) and a different number of resistors (R_L) coupled in parallel to convert the output current (out_m or out_n) into voltage and control the gain, as depicted in Figure 2. Finally, the two different outputs from the CS are used to provide distinct gains. The mathematical operation of the circuit is described as follows.

$$Sum = S \cdot (k_1 \cdot ch_1 + k_i \cdot ch_i + \cdots + k_n \cdot ch_n). \tag{3}$$

The coefficients k_i may be controlled in the readout circuit by tuning the SiPM bias voltage and the coefficient S is controlled at the summation element by selecting out_m or out_n as output. More specifically, out_m is used for the high gain (HG) output and out_n for the low gain (LG). Moreover, the sum block is configured with a double differential trans-impedance gain (Zt) by having a configurable resistor R_L with two possible values. Thus, the sum of signals can be performed with 4 total different gains.

The output voltage V_O of the current switch is connected to the PZ shaper (or can be bypassed) and then is provided at the output using the same differential driver implemented in the PACTA ASIC [49] with cable and transmission line driving capabilities. A differential voltage is provided at the output and thus common mode noise can be filtered by the common mode rejection of the data acquisition system in the measurements.

2.5. Individual Readout

The input stage provides different output currents where two of them are dedicated to the individual readout of each of the SiPMs connected to the ASIC. One of these currents is used to output the analog response of the SiPM in voltage mode using a single ended version of the differential driver implemented in the PACTA ASIC [49]. This driver presents a high slew rate and a low output impedance stage also with cable and transmission line driving capabilities.

Individual binary outputs are obtained using the other current from the readout stage, a shaper and a voltage comparator. Each channel delivers a binary signal encoding the amount of collected charge in the duration of a pulse using a non-linear Time Over Threshold (ToT) response. The voltage comparator structure is based on a preamplifier stage based on two differential amplifiers, a classical CMOS symmetric amplifier in an open loop configuration to work as a comparator and a digital buffer[58]. The buffer has enough drive strength in order to be connected to an FPGA or a micro-controller for digitization. The binary outputs are obtained using a programmable threshold in the discriminator with a 9 bit dynamic range and an LSB of 1.58 mV. The advantage of using a ToT readout is

that minimizes additional dedicated components (no ADC required) since digitization can be performed by Time to Digital Converters (TDCs) in an FPGA [59]. The fast shaping applied to the input pulse, also allows the possibility of photon counting. Lastly, the PZ cancellation can be used or bypassed by either the analog or the binary response.

2.6. MUSIC Specifications

This section describes the most significant characteristics of the MUSIC ASIC. The sum of signals presents a linear response in the whole dynamic range (15 bits), as depicted in Figure 5a for both the high gain (VoHG) and the low gain (VoLG) outputs. Observe that each sum output has an additional gain configuration referred as High Zt (high trans-impedance gain) and Low Zt (low trans-impedance gain) and both behave linearly. The single-ended channel has a linear response during the first half dynamic range (10 bits) and a non-linear in the second half, as illustrated in Figure 5b. The dynamic range of the individual response is increased when connecting the output of the chip to high impedance loads. The individual readout has also two trans-impedance gains.
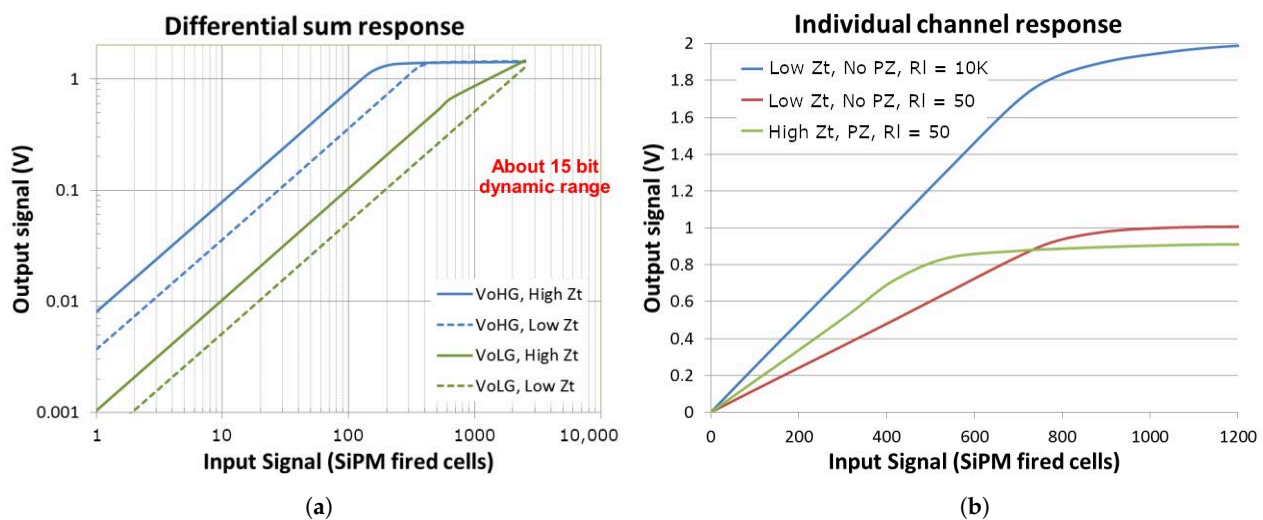

Figure 5. Dynamic Range and linearity of the analog functional modes. (**a**) Summation of 8 channels: Transient simulation using an input cell signal normalized to 12 µA current peak per cell. (**b**) Individual readout: Transient simulation using an input cell signal normalized to 8 µA current peak per cell.

Noise has been evaluated in terms of Equivalent Noise Charge (ENC). The ENC is computed by measuring the RMS noise present at the output and referring it to the input by dividing it by the measured impulse charge gain of the readout chain. The ENC of the summation and the analog individual response varying the input detector capacitance after 10 ns integration time is illustrated in Figure 6a,b respectively. Observe from Figure 3b, that most of the charge of a fast SiPM pulse affecting the SNR is located at the beginning of the sensor response and thus the ENC mostly depends on this fraction of time.

Figure 6a shows that the ENC increases with the input capacitance and the amount of active channels activated. For instance, considering a SiPM with a nominal gain of 2×10^6, a SNR of at least 5 can be achieved when summing 7 sensors with a detector capacitance of about 1 nF. Observe from Figure 6b the impact of the PZ cancellation on the ENC. SNR is slightly degraded for a small sensor capacitance due to the PZ shaper attenuates the signal. On the contrary, SNR is improved for a big sensor capacitance since the PZ filters the high frequency noise and thus ENC is limited, in this case, by the low frequency noise.
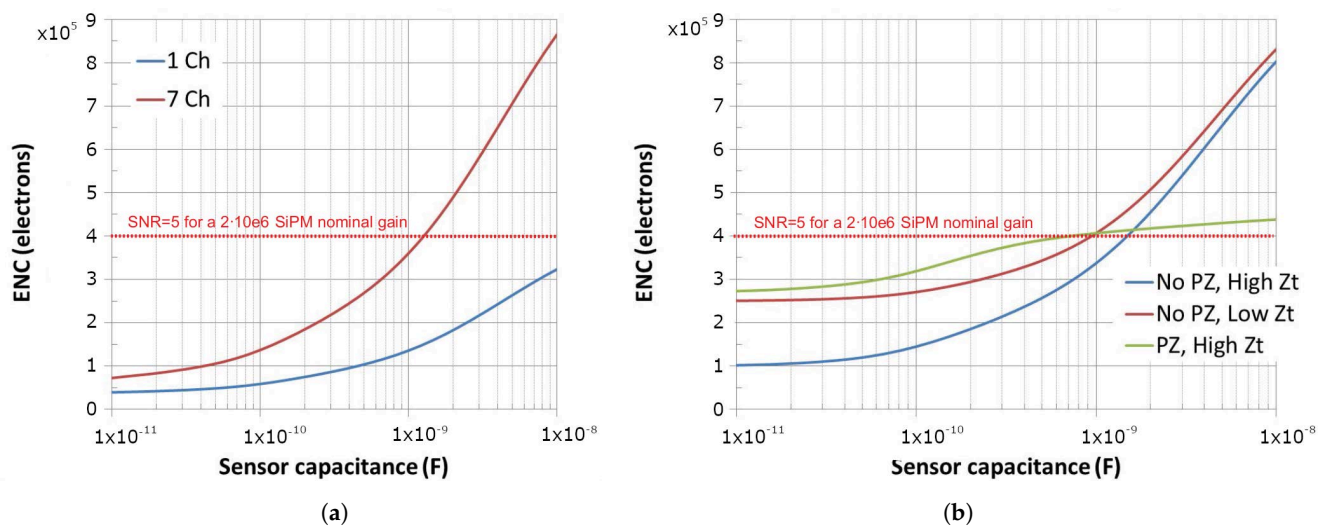
Figure 6. Equivalent Noise Charge (ENC) for different sensor capacitance after 10 ns integration time of the input signal. (**a**) Summation of the HG differential output for 1 and 7 channels. (**b**) Individual analog single ended response with and without PZ filter and using the high and low trans-impedance (Zt) gains.

Lastly, the binary output presents a very low noise at the comparator. More specifically, noise is close to 1 LSB (1.58 mV) of the comparator thresholds. As a summary, Table 1 details the main performance parameters of the MUSIC ASIC.

Table 1. Performances of the different functional modes. Note that the comparator noise is expressed in LSBs (1.58 mV).

Performance	Summation	Individual Analog	Individual Binary
Gain	HG:690 Ω/315 Ω LG:90 Ω/45 Ω	480 Ω/180 Ω	1 kΩ
GBW	500 MHz	150 MHz	>500 MHz
Dyn. Range	>15 bits	>10 bits	ToT
Output	Differential (×2)	Single Ended	CMOS
SNR (C_{det} = 1 nF)	>5	>5	-
Comp Noise	-	-	<1 LSB
Power	25 mW/ch	30 mW/ch	15 mW/ch

3. Methods

This section provides an overview of the experimental setups employed to evaluate the performance of the MUSIC. The Data Acquisition System (DAQ) is based on a Printed Circuit Board (PCB) basically containing the ASIC, connectors, power regulators, and an Altera Cyclone III FPGA. Moreover, it contains several pin sockets to place SiPM sensors of different sizes. For instance, the PCB can allocate up to 7 Hamamatsu SiPMs S13360-6050CS covering a nearly circular area similar to a PMT of 1 inch, as shown in Figure 7. This configuration will be employed to test the summation circuit. The FPGA is used to communicate with the ASIC via SPI in order to change any configuration register in the ASIC. The data are acquired directly via an oscilloscope.

The linearity test was performed using an electrical pulse injected directly into the MUSIC ASIC, as depicted in Figure 8. An arbitrary waveform generator (Tektronix AFG3252 240 MHz) that emulates the SiPM signal response of the Hamamatsu SiPM S13360-6050CS sends the pulse to a programmable attenuator (Agilent 11713B). By this means, it is possible to sweep a wide range of attenuation factors in order to study the behavior of the ASIC with several voltage amplitudes. This voltage signal is converted into current by placing a 510 Ohms resistor after the attenuator and before the ASIC. The amount of photoelectrons injected into the ASIC depending on the input current, can be calibrated by knowing the analog response of one photon using the MUSIC ASIC. The input current can be obtained

by dividing the output peak voltage of the analog response of one photon by the transimpedance gain of the ASIC. Lastly, the measurements were acquired with an Agilent MSO 9404A 4 GHz oscilloscope (20 GS/s).
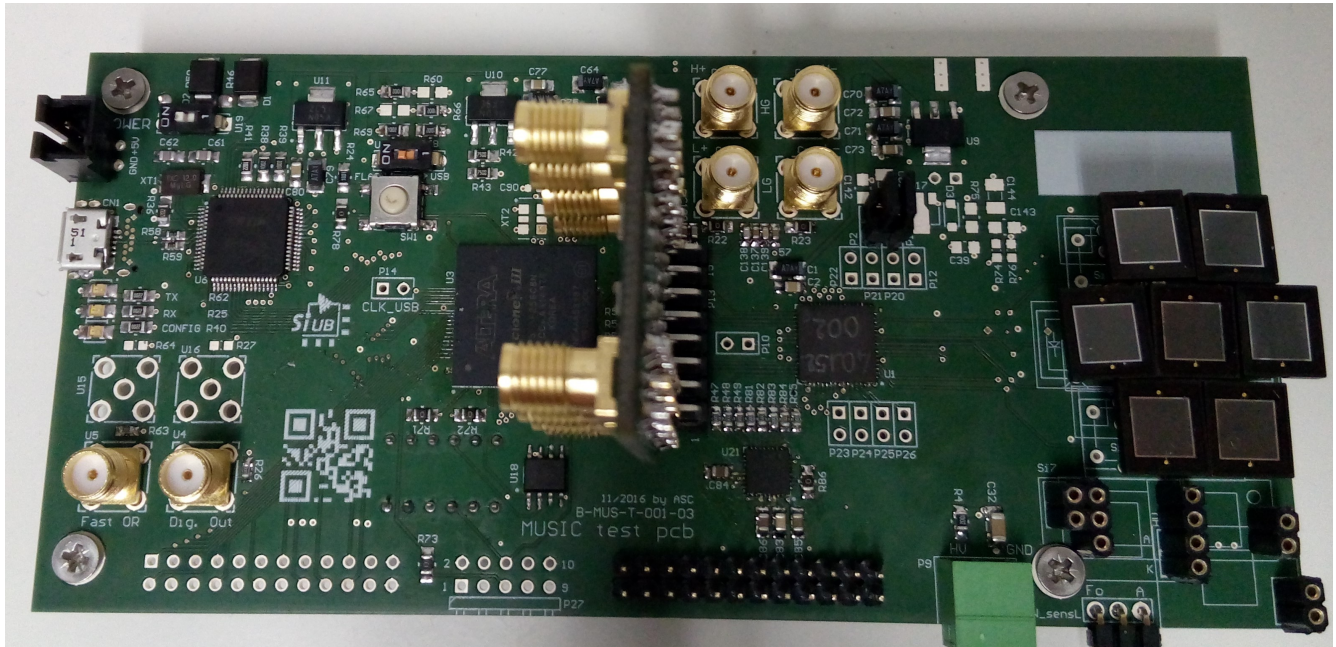

Figure 7. Printed Circuit Board (PCB) containing mainly the MUSIC ASIC, an Altera Cyclone III FPGA, power regulators, and connectors. It also illustrates how to connect 7 Hamamatsu SiPMs S13360−6050CS to show the performance of the summation circuit. The PCB measures 144.75×67.66 mm^2.
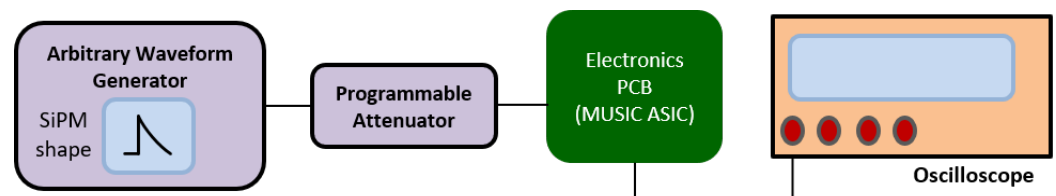

Figure 8. Schematic representation of the experimental setup used to evaluate the linearity of the energy measurement. The electronics are placed in a light tight box.

The experimental setup used to perform charge spectrum (finger-like plot) and SPTR (Single Photon Time Resolution) measurements is illustrated in Figure 9. An external trigger at 500 kHz sends a signal to both the laser driver and the oscilloscope. The laser driver sends a pulse to the laser (PicoQuant PDL 800-D laser at 635 nm and a tuned intensity level of 50% as per the optimal operating conditions specified in the user manual, jitter < 20 ps rms and 30 ps pulse width). The laser generates a red photon package that passes through a Single Mode Fiber (Throlabs 630A-FC SM) to a beam collimator. A few optical beam attenuators crystals are placed after the collimator to reduce the light intensity. Finally, the beam pulse arrives at a Thorlabs N-BK7 ground glass diffuser, spreading the light homogeneously over the sensors. All measurements were taken in an isolated light tight box and temperature was stabilized around 18 °C to avoid gain variations and reduce dark count noise.
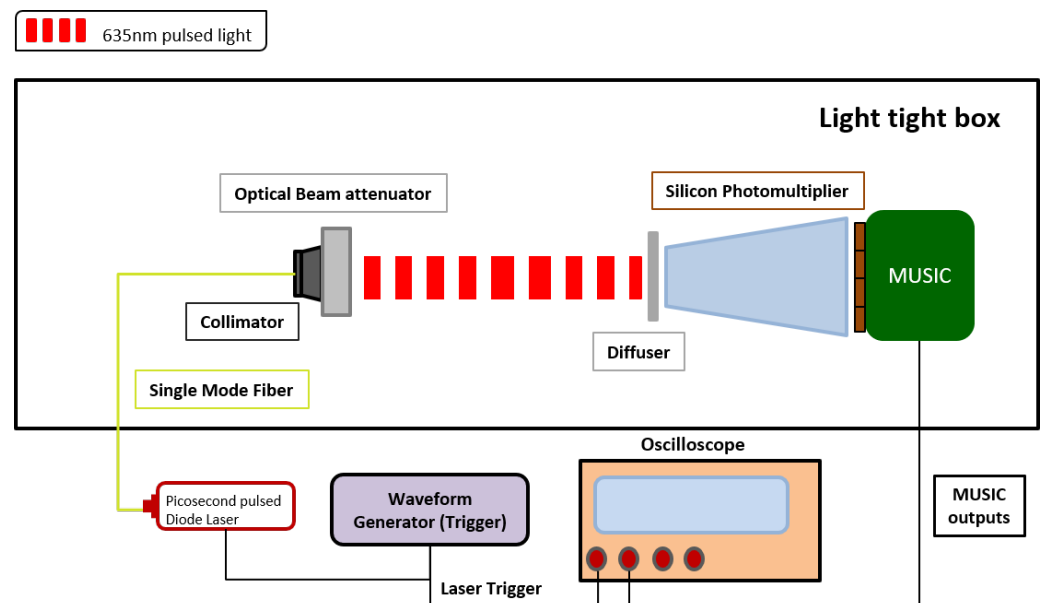
Figure 9. Schematic representation of the experimental setup using a red laser source for charge and single-photon time resolution (SPTR) measurements.

4. Experimental Test Results

This section provides experimental results of the different functional modes included in the ASIC. The MUSIC ASIC has been developed by using the AMS 0.35 μm SiGe BiCMOS technology.

4.1. Individual Analog Readout

The single-ended individual analog readout provides a SiPM response with an excellent SNR, even when the default configuration of the PZ cancellation is activated. Figure 10 shows the analog response of the Hamamatsu SiPM S13360-3075CS. The SiPM is illuminated at low light level conditions following a Poisson distribution with an average of a few photons. Discrete levels related to the number of fired cells can be easily distinguished in Figure 10a with a linear behavior of the peak amplitude with respect to the detected photons. Moreover, observe from Figure 10b that the charge histogram presents also a linear behavior with respect to the number of photons.
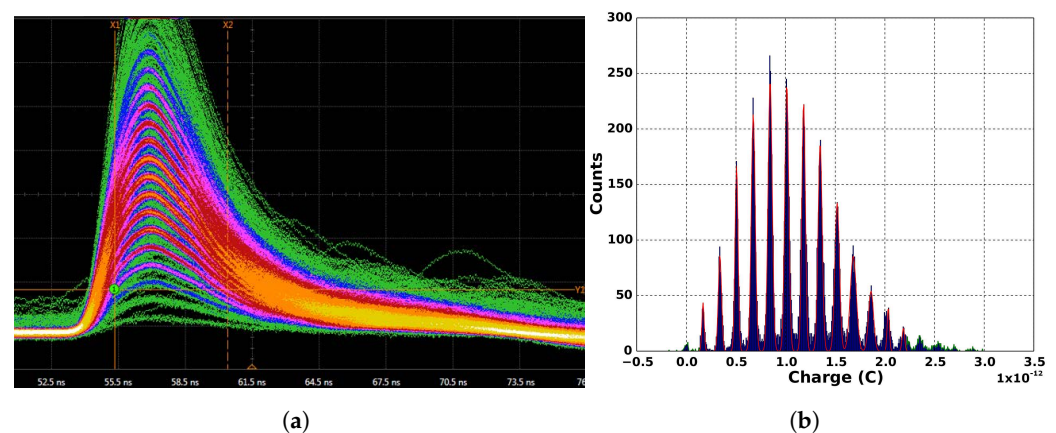

(**a**)

(**b**)

Figure 10. Individual analog output with the default PZ cancellation at low level illumination using the Hamamatsu SiPM S13360−3075CS at 5 V of over−voltage. (**a**) Analog output pulses with a FWHM of 5 ns; (**b**) Charge histogram.

The PZ cancellation narrows down the SIPM pulse providing an excellent resolution with a FWHM of ≈5 ns. Note that the FWHM of the SiPM input signal was higher than

100 ns. The SNR of the MUSIC ASIC allows a clear identification of more than 10 photon peaks in the charge spectrum, as depicted in Figure 10b. It is important to highlight that there exists a trade-off between SNR or amplitude and the resolution (FWHM) and thus the best PZ configuration will depend on the application and sensor.

Figure 11a shows the acquisition of several SiPMs with different detector capacitance (S13360-3050CS with 0.32 nF, S13360-6050CS with 1.28 nF and S14520-6050VE with 2.06 nF) with the same PZ cancellation. Photons can be perfectly identified with the S13360 series at 5 V of over-voltage. In contrast, the S14520 SiPM with this bigger capacitance, requires a larger over-voltage of about 7 V to distinguish the different photons when measuring the peak amplitude. Observe from Figure 11b that photons can be identified using the S14520-6050VE at 5 V of over-voltage when computing the charge histogram of the analog output. Therefore, the individual analog response is capable of processing SiPMs with a capacitance of ≈2 nF. However, it requires a larger over-voltage to distinguish them in terms of peak amplitude, at the expense of more cross-talk and dark count rate compared to the other sensors that can operate at lower over-voltages.
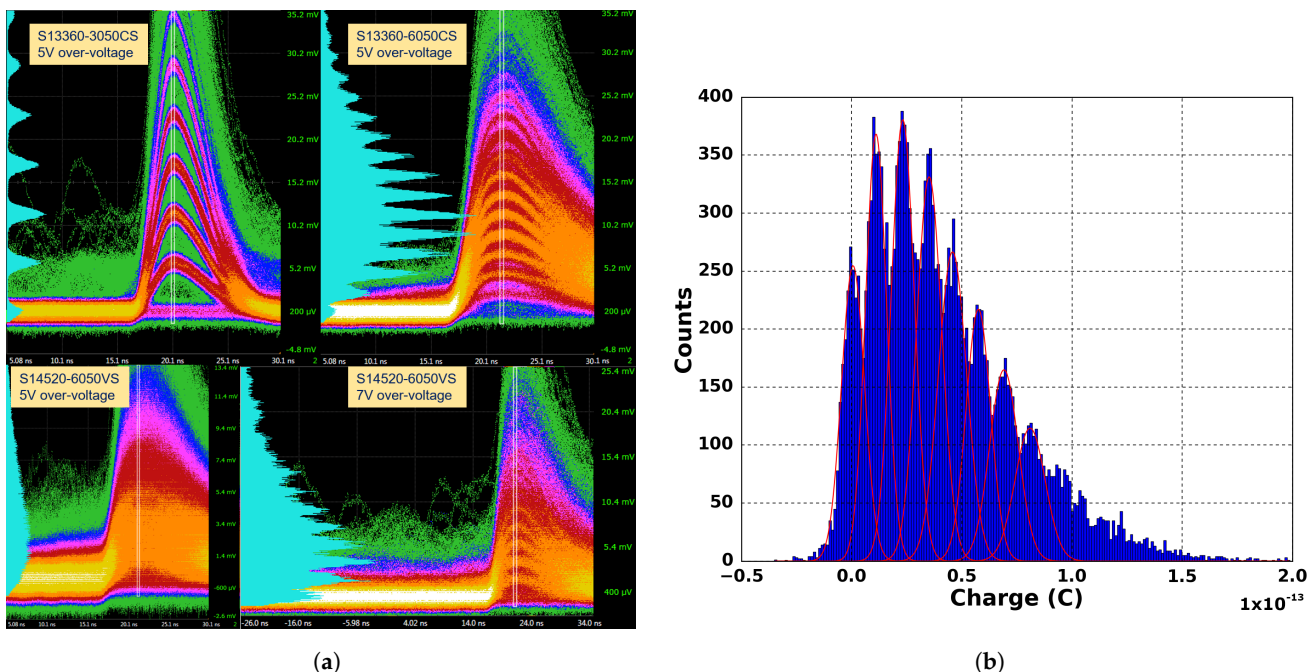

(**a**) (**b**)

Figure 11. MUSIC individual channel analog response for different SiPMs with PZ cancellation at low level illumination. (**a**) Analog output pulses and peak amplitude histogram for the Hamamatsu SiPMs S13360−3050CS, S13360−6050CS and S14520−6050VE at different over−voltages. (**b**) Charge histogram of the Hamamatsu SiPM S14520−6050VE at 5V of over−voltage.

4.2. Individual Binary Readout

An example of the binary outputs is shown in Figure 12 for the Hamamatsu SiPM S13360-3075CS. The SNR provided by MUSIC allows identifying the number of incident photons looking at the pulse width. The Single Photon Time Resolution (SPTR) of the combination of the SiPM and MUSIC can be measured by looking at the RMS spread of the delay between the leading edge of the laser trigger signal and the leading edge of the MUSIC discriminated output. Figure 12 illustrates the pulse width histogram of the discriminated signal and the delay distribution of the first photon to obtain the SPTR. The SPTR of the binary output with PZ cancellation is about 118 ps sigma at 5 V of over-voltage. Note that the measured SPTR is the combination of the jitter from the electronics, the SiPM and the laser.
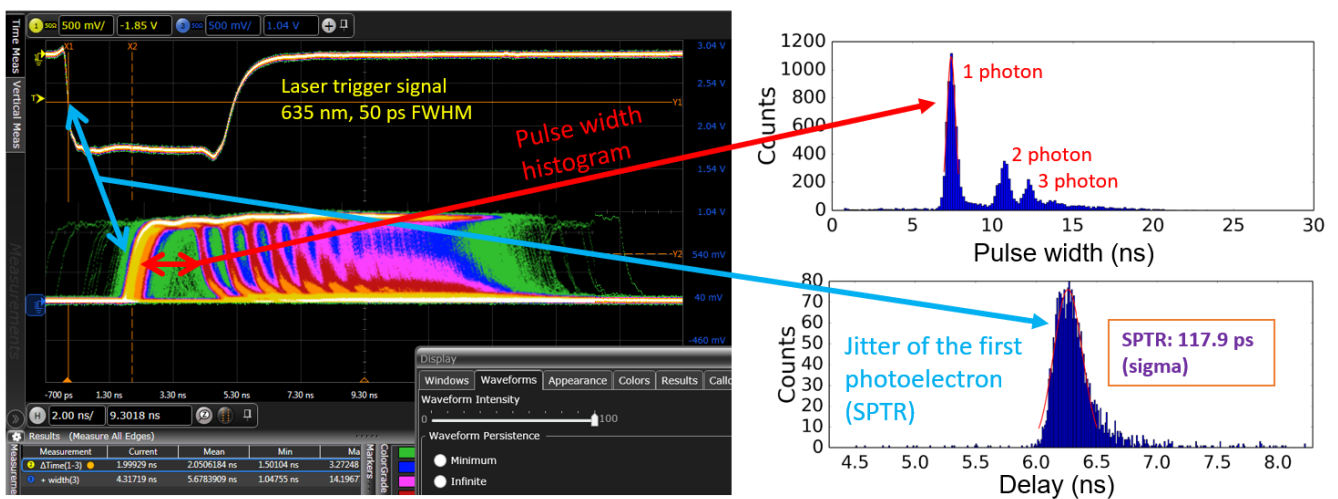
Figure 12. (**left**) MUSIC discriminated output with PZ cancellation and optimal threshold using the Hamamatsu SiPM S13360−3075CS at 5 V of over−voltage. (**Top-right**) Pulse width histogram of the discriminated. (**Bottom-right**) Delay distribution of the first photoelectron.

Single Photon Time Resolution as a function of over-voltage and different threshold levels (0.5 to 2.5 PEs or micro-cells) is depicted in Figure 13a (without PZ cancellation) and Figure 13b (with PZ cancellation). The SPTR deteriorates for higher over-voltages when PZ cancellation is not applied mainly due to the large tail of the SiPM signal (large FWHM) and the dark count rate pile-up. The employment of the PZ cancellation keeps lower the SPTR at higher over-voltages.
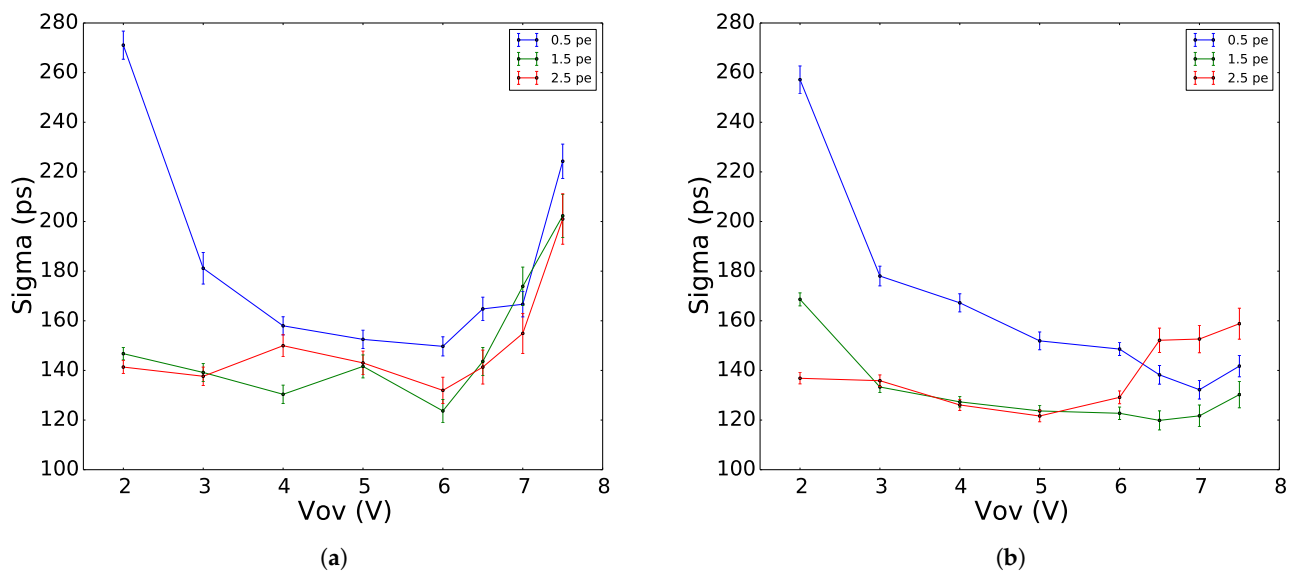

Figure 13. SPTR as a function of the over-voltage and different threshold levels using the Hamamatsu SiPM S13360−3075CS. (**a**) SPTR without PZ cancellation; (**b**) SPTR with PZ cancellation.

4.3. Analog Summation Readout

The summation circuit is evaluated using 7 Hamamatsu SiPMs S13360-6050CS covering a circular area similar to a PMT of 1 inch. The summation output pulse has a similar shape as the individual single-ended analog output (shown in Figure 10a), but in differential mode. Figure 14a illustrates the charge histogram of the high gain summation output at low light intensity when the adder activates only 1 channel whereas in Figure 14b the summation takes 7 channels. The input voltage of each readout channel, in other words, the anode voltage of each SiPM has been adjusted to equalize the over-voltage of each sensor

and thus minimizing gain variations between channels. Moreover, the PZ cancellation has been adjusted considering a trade-off between resolution and speed.

Figure 14a shows that the peaks in the charge histogram can be clearly identified when only one channel is processed. Figure 14b illustrates that photons can still be identified when summing 7 channels, despite being more affected by noise. The summation circuit adds the signal from each channel, but it also adds the noise contribution of each of them. Thus, the resultant noise is $\sqrt{7}$ times the noise of a single channel, in other words, $\sqrt{N}\sigma_i$, where N represents the number of channels added.
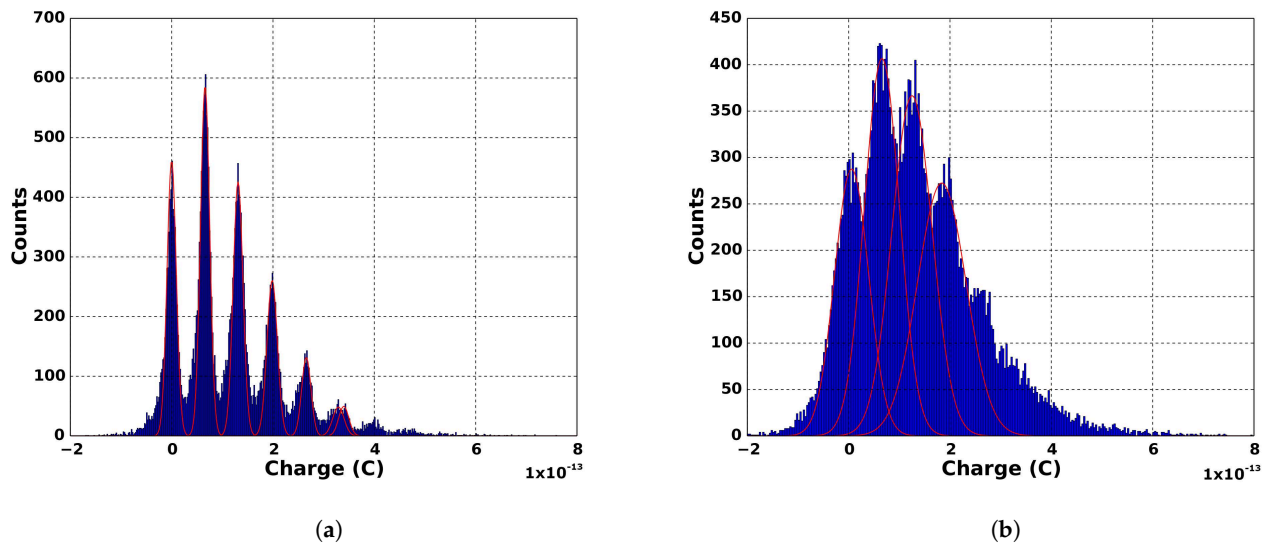

| (a) | (b) |

Figure 14. Charge distribution of the summation circuit with PZ cancellation using the Hamamatsu SiPM S13360−6050CS at 6V of over−voltage. (**a**) Summation of 1 channel; (**b**) Summation of 7 channels.

An electrical pulse that emulates the pulse shape of the Hamamatsu SiPM S13360-6050CS is injected into the ASIC to test the proper behavior of the summation circuit. Figure 15a (high gain output) and Figure 15b (low gain output) show the summation response of the MUSIC ASIC when activating a different number of channels. The same input signal is injected in each of the activated channels. These measurements show that the output peak voltage of n input channels is independent of the number of active channels for both gain configurations. Therefore, independently of the amount of signal received in each channel, the summation output will provide the sum of all of them following a linear behavior. These measurements were performed only up to 6 channels due to the test system did not allow to sum more signals. Although, the expected behavior for 8 channels is similar.
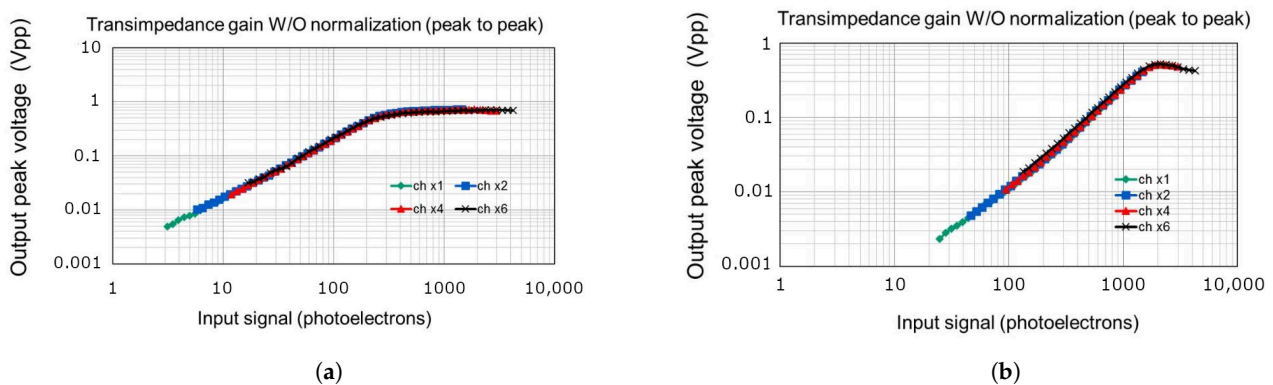

| (a) | (b) |

Figure 15. Summation of different amount of channels with PZ cancellation using the Hamamatsu SiPMs S13360−6050CS at 6 V of over−voltage. (**a**) High Gain output. (**b**) Low Gain output.

5. Discussion and Applications

Experimental measurements using the MUSIC ASIC showed that the summation feature can linearly add signals from different SiPMs and thus cover a large detection area. This unique feature makes it different from other ASICs in the literature that only provides the individual readout of each SiPM [44,49–51]. Moreover, the ASIC outputs the response of each channel in analog and binary mode. The analog response provides an output pulse with a FWHM between 5–10 ns. SPTR measurements performed using a Hamamatsu SiPM S13360-3075CS are around ≈118 ps sigma. Hence, the main target of this chip is fast applications employing detectors with large SiPM capacitance and/or requiring a timing resolution around 100 ps sigma [11,20,60–62].

MUSIC was designed for high speed applications, namely, cameras for Gamma-Imaging Atmospheric Cherenkov Telescopes (IACTs) (in summation [36] or in individual channel [63] mode), particle physics detectors, other Cherenkov or scintillator detectors (analog or photon-counting mode) or in general, applications where a large photo-detector area with good timing and fast shaping is required. More specifically, it will enable to substitute multi-anode PMTs or PMTs with a large photo-detection area by SiPM arrays. For instance, 1-inch diameter PMTs could be substituted for a self assembled matrix of 7 small SiPMs measuring 6×6 mm^2 in order to cover the same pixel's detection area. The MUSIC ASIC configured in the summation mode, can sum the input currents of each pixel into one single output as the one provided by a PMT readout.

Several applications where the MUSIC ASIC have been employed are discussed in this section. For instance, MUSIC has been considered and experimentally evaluated to be employed in the timing detector of the SHIP experiment [11,60]. This experiment is a new general-purpose fixed target facility at the European Council for Nuclear Research (CERN) Super Proton Synchrotron (SPS) to search for hidden particles as predicted by a very large number of recently elaborated models of hidden sectors. In this project, an array of 8 Hamamatsu SiPMs S13360-6050PE was directly coupled to each end of several long plastic scintillator bars. The signal was processed with the summation capability of the MUSIC ASIC and a time resolution below 100 ps for the incoming particles was achieved [60].

A similar approach was used for the Surrounding Background Tagger of the SHiP experiment [64]. They employed the summation feature to read the signal from an array of 8 Hamamatsu S13360-6050PE SiPMs (covering a similar area of a PMT) coupled to a liquid-scintillator detector module of $50 \times 50 \times 30$ cm^3 volume and one wavelength-shifting optical module. Photo detection efficiencies of at least 99.7% for a threshold of five photoelectrons were accomplished.

MUSIC was also considered for the ND280 near ToF detector of the T2K experiment in J-PARC [11]. This experiment aimed to measure the energy spectrum, flavor content and neutral and charged current interaction rates of the non-oscillated neutrino beam. This information can be used to predict the non-oscillated interaction rates at Super-Kamiokande. The purpose of the ToF detector is the determination of the direction of particles (inside or outside the target) which are products of beam-neutrino interactions. The resolution required for this system is between 100–200 ps which can be obtained with the MUSIC ASIC [11,60].

MUSIC was also used as a beam loss monitor (BLM) [65] in combination with scintillator fibers to compute the rate of radiation losses in the whole ring or by regions at the ALBA synchrotron facility [66]. The beam loss deposition was absorbed by scintillation fibers and the light generated was collected at both ends by two Hamamatsu SiPMs S13360-3050CS, as illustrated in Figure 16a. Then, sensor outputs were processed by the individual binary channels of the MUSIC ASIC and sent to an Altera Cyclone III FPGA to determine the arrival time of each photon. The binary output was digitized using an FPGA-based time to digital converter (TDC) with 40 ps sigma time resolution. A photon counting implemented in the FPGA was used to capture variations in rate during the operation of the accelerator at the ALBA facility. Additionally, a Time of Fight measurement was performed by computing

the difference in arrival times of the photons at both ends of the scintillation fibers. A 20 cm spatial resolution was measured using a 4 m scintillation fiber, as shown in Figure 16b.
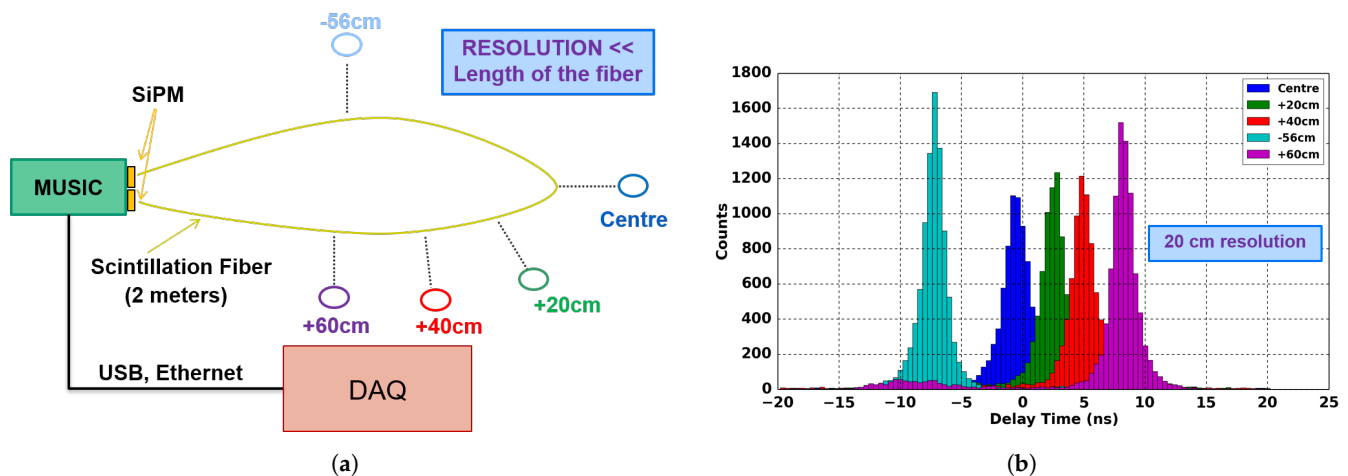

Figure 16. Beam Loss Monitor (BLM) employing the MUSIC ASIC, a scintillator fiber and two Hamamatsu SiPMs S13360−3050CS. (**a**) BLM diagram showing different locations where a radioactive source (gamma photons) was placed to interact with the plastic fiber; (**b**) CTR with PZ cancellation.

The authors in [20], employed the MUSIC ASIC to study its feasibility in a Single Photon Emission Computed Tomography (SPECT) scanner. They built a micro-camera consisting of a $40 \times 40 \times 8$ mm^3 NaI(Tl) crystal coupled to 64 SiPMs distributed in a matrix of 8×8 pixels. The 32 SiPMs located in the center of the matrix were read in groups of 8 SiPMs with four MUSIC ASICs using the summation mode. This camera achieved an intrinsic spatial resolution of ≈ 2 mm and an energy resolution of $\approx 11.6\%$ at 140 keV when reconstructing images of a liquid radioactive solution of ^{99m}Tc in a central region of 15×15 mm^2.

Another application under investigation is the employment of the MUSIC ASIC in muon imaging and tracking applications as a Cherenkov-Tag detector [67] and a non-invasive scanner for cargo containers [68]. Muons passing through a container used in cargo transportation to be inspected are tracked above and below the volume using a few modules of several strips of extruded plastic scintillators. The Cherenkov-Tag detector is based on the directionality of Cherenkov light produced by the muons in a transparent material that works as a radiator. The MUSIC ASIC connected to several SiPMs attached to the ends of the scintillator bars or to one face of the radiator material has the right specifications to detect scintillation or Cherenkov light also in single-photon counting condition.

An SiPM readout based on the MUSIC ASIC is currently used to develop a Cherenkov telescope for the detection of ultrahigh energy cosmic rays, more specifically, the observation of neutrinos with energies above 10^7 GeV. This Cherenkov Telescope is planned to be deployed on the Extreme Universe Space Observatory Super Pressure Balloon 2 (EUSO-SPB2) as a precursor experiment to the proposed Probe of Extreme Multi-Messenger Astrophysics (POEMMA) [62]. The MUSIC circuit is also under test for a custom system for neuro-biological applications with a Fluorescence Lifetime Imaging technique, similar to the one presented in [69], but using SiPMs.

Several studies for gamma-ray telescopes have been carried out using the MUSIC electronics for CTA. MUSIC was one of the candidates to be employed in the Small Size Telescopes (SSTs) [70], but finally the camera implementation proposing the MUSIC ASIC as the readout electronics of the SiPMs were discarded. The upgrade of the Large Size Telescopes (LSTs) based on SiPMs instead of PMTs is currently being studied [4,71]. MUSIC is being evaluated as a candidate due to the possibility to readout large SiPM pixels with the summation mode [61].

Lastly, the summation concept presented in the MUSIC circuit, has been implemented in a new ASIC, referred to as FASTIC (available during 2021). This ASIC was developed in a 65 nm technology node and provides the readout of 8 channels as the summation of the inputs in two groups of 4 channels. It also reads each channel individually and accepts both positive and negative polarity input signals. This ASIC performs a measurement of the arrival time of the photons (with better time resolution) using a non-Linear ToT technique and includes a linear ToT for energy measurement, as implemented in the HRFlexToT ASIC [46,72,73]. Besides the binary output encoding the time and energy response, the FASTIC also provides the response of each output in analog mode using a capacitive driver. All these functionalities are performed with a power consumption of about 10 mW/channel.

6. Conclusions

An 8-channel ASIC, referred to as MUSIC, for SiPM anode readout in large detection areas was proposed. MUSIC includes three main operational modes: (1) SiPM pixel summation in differential mode, (2) 8 individual single ended analog channels, and (3) 8 individual binary outputs. Additionally, a trigger pulse is provided by performing the logic OR operation between the binary signals. The MUSIC ASIC is designed for high speed sampling. It achieves a pulse width between 5 ns and 10 ns while keeping a good SNR at the Single Photo Electron level. The binary output presents a Single Photon Time Resolution around 118 ps using a Hamamatsu SiPM S13360-3075CS which enables the possibility to use this ASIC in some timing detectors. The summation capability of the ASIC is proven even when summing 7 channels at the same time. The MUSIC chip has been experimentally tested in particle physics detectors requiring Time of Flight measurements, in Cherenkov telescopes, in muon imaging as a Cherenkov-Tag ToF detector, as a proof-of-concept SPECT camera, as a Beam Loss Monitor and in Fluorescence Lifetime Imaging. In conclusion, the summation concept has been proven in the laboratory and experimentally demonstrated in several applications, such as a scintillator ToF detector or a SPECT camera, and thus showing the potential capabilities of this technique to process sensors with large detection areas.

Data Availability Statement: The ASIC presented in this study is available through SCIENTIFICA INTERNATIONAL, S.L.U. Check the website: https://www.scientifica.es/, accessed on 1 January 2021.

Conflicts of Interest: The authors declare no conflict of interest.

References

1. Renker, D.; Lorenz, E. Advances in solid state photon detectors. *J. Instrum.* **2009**, *4*, P04004.. [CrossRef]
2. Del Guerra, A.; Belcari, N.; Giuseppina Bisogni, M.; Corsi, F.; Foresta, M.; Guerra, P.; Marcatili, S.; Santos, A.; Sportelli, G. Silicon Photomultipliers (SiPM) as novel photodetectors for PET. *Nucl. Instrum. Methods Phys. Res. Sect. A* **2011**, *648*, S232–S235. [CrossRef]
3. Picatoste, E.; Gascón, D.; Abelln, C.; Lefrançois, J.; Machefert, F.; Duarte, O.; Grauges, E.; Garrido, L.; Vilasis, X. Low noise front end ICECAL ASIC for the Upgrade of the LHCb Calorimeter. *J. Instrum.* **2012**, *7*, C01080. [CrossRef]
4. Perennes, C.; Doro, M.; Corti, D.; Lessio, L.; Mallamaci, M.; Mariotti, M.; Rando, R.; Salmaso, I. Optical feasibility of an upgrade of the CTA LST camera to SiPM. *Nucl. Instrum. Methods Phys. Res. Sect. A* **2020**, *984*, 164485. [CrossRef]
5. Guz, Y. The Phase 2 Upgrade of the LHCb Calorimeter system. *J. Instrum.* **2020**, *15*, C09046–C09046. [CrossRef]

6.   Jha, A.K.; van Dam, H.T.; Kupinski, M.A.; Clarkson, E. Simulating Silicon Photomultiplier Response to Scintillation Light. *IEEE Trans. Nucl. Sci.* **2013**, *60*, 336–351. [CrossRef] [PubMed]

7.   Simon, F. Silicon photomultipliers in particle and nuclear physics. *Nucl. Instrum. Methods Phys. Res. Sect. A* **2019**, *926*, 85–100. [CrossRef]

8.   Mazorra, J.; Chanal, H.; Comerma, A.; Gascón, D.; Gómez, S.; Han, X.; Pillet, N.; Vandaele, R. PACIFIC: The readout ASIC for the SciFi Tracker of the upgraded LHCb detector. *J. Instrum.* **2016**, *11*, C02021–C02021. [CrossRef]

9.   de Cos, J.M.; Chanal, H.; Comerma Montells, A.; Gascón Fora, D.; Gómez Fernández, S.; Han, X.; Pillet, N.; Vandaelle, R. PACIFIC: SiPM readout ASIC for LHCb upgrade. *Nucl. Instrum. Methods Phys. Res. Sect. A* **2018**, *912*, 354–358. [CrossRef]

10.   Gundacker, S.; Acerbi, F.; Auffray, E.; Ferri, A.; Gola, A.; Nemallapudi, M.V.; Paternoster, G.; Piemonte, C.; Lecoq, P. State of the art timing in TOF-PET detectors with LuAG, GAGG and L(Y)SO scintillators of various sizes coupled to FBK-SiPMs. *J. Instrum.* **2016**, *11*, P08008. [CrossRef]

11.   Korzenev, A.; Serra, N.; Mermod, P.; Gascon, D.; Sgalaberna, D.; Gomez, S.; Blondel, A.; Favre, Y.; Dätwyler, A.; Noah, E.; et al. Application of SiPM arrays for the readout of a scintillator based time-of-flight detector. In Proceedings of the EPS Conference on High Energy Physics, Venice, Italy, 5–12 July 2017.

12.   Cassina, L. Photodetectors and front-end electronics for the LHCb RICH upgrade. *Nucl. Instrum. Methods Phys. Res. Sect. A* **2016**, *876*, 217–220. [CrossRef]

13.   Fiorini, M. The upgrade of the LHCb RICH detectors. *Nucl. Instrum. Methods Phys. Res. Sect. A* **2020**, *952*, 161688. [CrossRef]

14.   Krennrich, F.; Akerlofb, C.W.; Buckley, J.H.; Buss, J.; Cawley, M.F.; Catanese, M.A.; Connaughton, V.; Fegan, D.J.; Finley, J.P.; Gaidos, J.A.; et al. Stereoscopic observations of gamma rays at the Whipple observatory. *Astropart. Phys.* **1998**, *8*, 213–221. [CrossRef]

15.   The CTA Consortium. Introducing the CTA concept. *Astropart. Phys.* **2013**, *43*, 3–18. [CrossRef]

16.   Aharonian, F.A.; Hofmann, W.; Konopelko, A.K.; Völk, H.J. The potential of ground based arrays of imaging atmospheric Cherenkov telescopes. I. Determination of shower parameters. *Astropart. Phys.* **1997**, *6*, 343–368. [CrossRef]

17.   Lecoq, P. Pushing the Limits in Time-of-Flight PET Imaging. *IEEE Trans. Radiat. Plasma Med. Sci.* **2017**, *1*, 473–485. [CrossRef]

18.   Gundacker, S.; Martinez Turtos, R.; Kratochwil, N.; Pots, R.H.; Paganoni, M.; Lecoq, P.; Auffray, E. Experimental time resolution limits of modern SiPMs and TOF-PET detectors exploring different scintillators and Cherenkov emission. *Phys. Med. Biol.* **2020**, *65*, 25001. [CrossRef] [PubMed]

19.   Carminati, M.; Fiorini, C. Challenges for Microelectronics in Non-Invasive Medical Diagnostics. *Sensors* **2020**, *20*, 3636. [CrossRef] [PubMed]

20.   Guberman, D.; Paoletti, R.; Rugliancich, A.; Wunderlich, C.; Passeri, A. Large-Area SiPM Pixels (LASiPs): A cost-effective solution towards compact large SPECT cameras. *Phys. Med.* **2021**, *82*, 171–184. [CrossRef]

21.   Gascon, D.; Chanal, H.; Comerma, A.; Gomez, S.; Han, X.; Mazorra, J.; Mauricio, J.; Pillet, N.; Yengui, F.; Vandaele, R. PACIFIC: A 64-channel ASIC for scintillating fiber tracking in LHCb upgrade. *J. Instrum.* **2015**, *10*, C04030–C04030. [CrossRef]

22.   The CTA Consortium. Design concepts for the Cherenkov Telescope Array CTA: An advanced facility for ground-based high-energy gamma-ray astronomy. *Exp. Astron.* **2011**, *32*, 193–316. [CrossRef]

23.   Hammamatsu Photonics K.K. Electron Tube Division. *Photomultipliers Tubes, Basics and Applications*; Hammamatsu: Tokoyo, Japan, 2006.

24.   Saveliev, V.; Golovin, V. Silicon avalanche photodiodes on the base of metal-resistor-semiconductor (MRS) structures. *Nucl. Instrum. Methods Phys. Res. Sect. A* **2000**, *442*, 223–229. [CrossRef]

25.   Gundacker, S.; Heering, A. The silicon photomultiplier: Fundamentals and applications of a modern solid-state photon detector *Phys. Med. Biol.* **2020**, *65*, 17–18. [CrossRef]

26.   Bisogni, M.G.; Morrocchi, M. Development of analog solid-state photo-detectors for Positron Emission Tomography. *Nucl. Instrum. Methods Phys. Res. Sect. A* **2016**, *809*, 140–148. [CrossRef]

27.   Eckert, P.; Schultz-Coulon, H.C.; Shen, W.; Stamen, R.; Tadday, A. Characterisation studies of silicon photomultipliers. *Nucl. Instrum. Methods Phys. Res. Sect. A* **2010**, *620*, 217–226. [CrossRef]

28.   Otte, A.N. SiPM's a very brief review. In Proceedings of the International Conference on New Photo-Detectors, Troitsk, Russia, 6–9 July 2015, doi:10.22323/1.252.0001. [CrossRef]

29.   Acerbi, F.; Gundacker, S. Understanding and simulating SiPMs. *Nucl. Instrum. Methods Phys. Res. Sect. A* **2019**, *926*, 16–35. [CrossRef]

30.   Sánchez, D.; Gómez, S.; Fernández-Tenllado, J.M.; Ballabriga, R.; Michael, C.; Gascón, D. Multimodal Simulation of Large Area Silicon Photomultipliers for Time Resolution Optimization. *Nucl. Instrum. Methods Phys. Res. Sect. A* **2021**, *1001*, 165247. [CrossRef]

31.   Cova, S.; Ghioni, M.; Lacaita, A.; Samori, C.; Zappa, F. Avalanche photodiodes and quenching circuits for single-photon detection. *Appl. Opt.* **1996**, *35*, 1956. [CrossRef]

32.   Otte, N. The Silicon Photomultiplier—A new device for High Energy Physics, Astroparticle Physics, Industrial and Medical Applications. In Proceedings of the SNIC symposium (SLAC), Stanford, CA, USA, 3–6 April 2006; pp. 1–9.

33.   Buzhan, P.; Dolgoshein, B.; Filatov, L.; Ilyin, A.; Kantzerov, V.; Kaplin, V.; Karakash, A.; Kayumov, F.; Klemin, S.; Popova, E.; et al. Silicon photomultiplier and its possible applications. *Nucl. Instrum. Methods Phys. Res. Sect. A* **2003**, *504*, 48–52. [CrossRef]

34. Seifert, S.; Van Dam, H.T.; Huizenga, J.; Vinke, R.; Dendooven, P.; Löhner, H.; Schaart, D.R. Simulation of silicon photomultiplier signals. *IEEE Trans. Nucl. Sci.* **2009**, *56*, 3726–3733. [CrossRef]

35. Marano, D.; Belluso, M.; Bonanno, G.; Billotta, S.; Grillo, A.; Garozzo, S.; Romeo, G.; Catalano, O.; La Rosa, G.; Sottile, G.; et al. Silicon photomultipliers electrical model extensive analytical analysis. *IEEE Trans. Nucl. Sci.* **2014**, *61*, 23–34. [CrossRef]

36. Rando, R.; Corti, D.; Dazzi, F.; De Angelis, A.; Dettlaff, A.; Dorner, D.; Fink, D.; Fouque, N.; Grundner, F.; Haberer, W.; et al. Silicon Photomultiplier Research and Development Studies for the Large Size Telescope of the Cherenkov Telescope Array. In Proceedings of the 34th International Cosmic Ray Conference (ICRC 2015), The Hague, The Netherlands, 30 July–6 August **2015**, doi:10.22323/1.236.0940. [CrossRef]

37. Piemonte, C. A new Silicon Photomultiplier structure for blue light detection. *Nucl. Instrum. Methods Phys. Res. Sect. A* **2006**, *568*, 224–232. [CrossRef]

38. Biteau, J.; Chinn, D.; Dang, D.; Doyle, K.; Johnson, C.A.; Williams, D.A. Performance of Silicon Photomultipliers for the Dual-Mirror Medium-Sized Telescopes of the Cherenkov Telescope Array. In Proceedings of the 34th International Cosmic Ray Conference (ICRC2015), The Hague, The Netherlands, 30 July–6 August 2015, doi:10.22323/1.236.0963. [CrossRef]

39. Hamamatsu Photonics K.K. S13360 Series—MPPCs for Precision Measurement. Available online: https://www.hamamatsu.com/resources/pdf/ssd/s13360_series_kapd1052e.pdf (accessed on 1 March 2021).

40. Gola, A.; Acerbi, F.; Capasso, M.; Marcante, M.; Mazzi, A.; Paternoster, G.; Piemonte, C.; Regazzoni, V.; Zorzi, N. NUV-Sensitive Silicon Photomultiplier Technologies Developed at Fondazione Bruno Kessler. *Sensors* **2019**, *19*, 308. [CrossRef]

41. Rivetti, A. *CMOS: Front-End Electronics for Radiation Sensors*; CRC Press: Boca Raton, FL, USA, 2015; pp. 1–683. [CrossRef]

42. Ciciriello, F.; Corsi, F.; Licciulli, F.; Marzocca, C.; Matarrese, G. Time performance of voltage-mode vs current-mode readouts for SiPM's. In Proceedings of the 2015 6th IEEE International Workshop on Advances in Sensors and Interfaces, IWASI 2015, Gallipoli, Italy, 18–19 June 2015; pp. 249–253. [CrossRef]

43. Fernandez-Tenllado, J.M.; Ballabriga, R.; Campbell, M.; Gascon, D.; Gomez, S.; Mauricio, J. Optimal design of single-photon sensor front-end electronics for fast-timing applications. In Proceedings of the IEEE Nuclear Science Symposium and Medical Imaging Conference, NSS/MIC 2019, Manchester, UK, 26 October–2 November 2019. [CrossRef]

44. Fleury, J.; Callier, S.; De La Taille, C.; Seguin, N.; Thienpont, D.; Dulucq, F.; Ahmad, S.; Martin, G. Petiroc and Citiroc: Front-end ASICs for SiPM read-out and ToF applications. *J. Instrum.* **2014**, *9*, C01049. [CrossRef]

45. Nadig, V.; Weissler, B.; Radermacher, H.; Schulz, V.; Schug, D. Investigation of the Power Consumption of the PETsys TOFPET2 ASIC. *IEEE Trans. Radiat. Plasma Med. Sci.* **2020**, *4*, 378–388. [CrossRef]

46. Sanchez, D.; Gomez, S.; Mauricio, J.; Freixas, L.; Sanuy, A.; Guixe, G.; Lopez, A.; Manera, R.; Marın, J.; Perez, J.M.; et al. HRFlexToT: A High Dynamic Range ASIC for Time-of-Flight Positron Emission Tomography. *IEEE Trans. Radiat. Plasma Med. Sci.* **2021**. [CrossRef]

47. Chen, H.; Briggl, K.; Fischer, P.; Gil, A.; Harion, T.; Munwes, Y.; Ritzert, M.; Schimansky, D.; Schultz-Coulon, H.C.; Shen, W.; et al. A dedicated readout ASIC for Time-of-Flight Positron Emission Tomography using Silicon Photomultiplier (SiPM). In Proceedings of the 2014 IEEE Nuclear Science Symposium and Medical Imaging Conference, NSS/MIC 2014, Seattle, WA, USA, 8–15 November 2016. [CrossRef]

48. Garutti, E. Silicon Photomultipliers for High Energy Physics Detectors. *J. Instrum.* **2011**, *6*, C10003. [CrossRef]

49. Sanuy, A.; Gascon, D.; Paredes, M.; Garrido, L.; Ribó, M.; Sieiro, J. Wideband (500 MHz) 16 bit dynamic range current mode PreAmplifier for the CTA cameras (PACTA). *J. Instrum.* **2012**, *7*, C01100. [CrossRef]

50. Anghinolfi, F.; Jarron, P.; Martemiyanov, A.N.; Usenko, E.; Wenninger, H.; Williams, M.C.S.; Zichichid, A. NINO: An ultra-fast and low-power front-end amplifier/discriminator ASIC designed for the multigap resistive plate chamber. *Nucl. Instrum. Methods Phys. Res. Sect. A* **2004**, *533*, 183–187. [CrossRef]

51. Gundacker, S.; Auffray, E.; Frisch, B.; Jarron, P.; Knapitsch, A.; Meyer, T.; Pizzichemi, M.; Lecoq, P. Time of flight positron emission tomography towards 100ps resolution with L(Y)SO: An experimental and theoretical analysis. *J. Instrum.* **2013**, *8*. [CrossRef]

52. Weeroc. Available online: https://www.weeroc.com/products/see-catalogue (accessed on 1 March 2021).

53. Gomez, S.; Gascon, D.; Fernández, G.; Sanuy, A.; Mauricio, J.; Graciani, R.; Sanchez, D. MUSIC: An 8 channel readout ASIC for SiPM arrays. In Proceedings of the SPIE 9899, Optical Sensing and Detection IV, Brussels, Belgium, 3–7 April 2016; Volume 9899.

54. Gascon, D.; Gomez, S.; Mauricio, J. EP3356903: Summation for Multi-Channel Photomultiplier Array Signals. Available online: https://patentscope.wipo.int/search/en/detail.jsf?docId=WO2017055477 (accessed on 1 March 2021).

55. Ramirez-Angulo, J.; Carvajal, R.G.; Torralba, A. Low Supply Voltage High-Performance CMOS Current Mirror With Low Input and Output Voltage Requirements. *IEEE Trans. Circuits Syst. Express Briefs* **2004**, *51*, 124–129. [CrossRef]

56. Laker, K.R.; Sansen, W.M.C. *Design of Analog Integrated Circuits and Systems*; McGraw-Hill: New York, NY, USA, 1994.

57. Park, S.M.; Toumazou, C. Low noise current-mode CMOS transimpedance amplifier for giga-bit optical communication. In Proceedings of the 1998 IEEE International Symposium on Circuits and Systems (Cat. No.98CH36187), ISCAS'98, Monterey, CA, USA, 31 May–3 June 1998; Volume 1, pp. 293–296. [CrossRef]

58. Sansen, W.M.C. *Analog Design Essentials*, 1st ed.; Springer: Berlin/Heidelberg, Germany, 2006; Volume 859.

59. Menninga, H.; Favi, C.; Fishburn, M.W.; Charbon, E. A multi-channel, 10ps resolution, FPGA-based TDC with 300MS/s throughput for open-source PET applications. In Proceedings of the 2011 IEEE Nuclear Science Symposium Conference Record, Valencia, Spain, 23–29 October 2011; pp. 1515–1522. [CrossRef]

60. Betancourt, C.; Blondel, A.; Brundler, R.; Dätwyler, A.; Favre, Y.; Gascon, D.; Gomez, S.; Korzenev, A.; Mermod, P.; Noah, E.; et al. Application of large area SiPMs for the readout of a plastic scintillator based timing detector. *J. Instrum.* **2017**, *12*, P11023. [CrossRef]

61. Berti, A.; Chiavassa, A.; Corti, D.; Depaoli, D.; Di Pierro, F.; Lessio, L.; Mallamaci, M.; Mariotti, M.; Perennes, C.; Rando, R.; et al. Development and test of a SiPM cluster for a SiPM version of the Cherenkov Telescope Array LST camera. *Nucl. Instrum. Methods Phys. Res. Sect. A* **2020**, *982*, 164373. [CrossRef]

62. Otte, A.N.; Gazda, E.; Judd, E.; Krizmanic, J.F.; Kutzenzov, E.; Matamala, O.R.; Reardon, P.J.; Wiencke, L. Development of a Cherenkov Telescope for the Detection of Ultrahigh Energy Neutrinos with EUSO-SPB2 and POEMMA. *arXiv* **2019**, arXiv:1907.08728.

63. Daniel, M.K.; White, R.J.; Berge, D.; Buckley, J.; Chadwick, P.M.; Cotter, G.; Funk, S.; Greenshaw, T.; Hidaka, N.; Hinton, J.; et al. A Compact High Energy Camera for the Cherenkov Telescope Array. *arXiv* **2013**, arXiv:1307.2807.

64. Ehlert, M.; Hollnagel, A.; Korol, I.; Korzenev, A.; Lacker, H.; Mermod, P.; Schliwinski, J.; Shihora, L.; Venkova, P.; Wurm, M. Proof-of-principle measurements with a liquid-scintillator detector using wavelength-shifting optical modules. *J. Instrum.* **2019**, *14*, P03021. [CrossRef]

65. Venturini, G.G. Characterization of a wide dynamic-range, radiation-tolerant charge-digitizer asic for monitoring of beam losses. In Proceedings of the International Beam Instrumentation Conference (IBIC), Tsukuba, Japan, 1–4 October 2012. Available online: https://accelconf.web.cern.ch/IBIC2012/papers/mopa12.pdf (accessed on 1 March 2021).

66. ALBA Synchrotron. Available online: https://www.cells.es/es/ (accessed on 1 March 2021).

67. Gallo, G.; Lo Presti, D.; Bonanno, D.L.; Bonanno, G.; La Rocca, P.; Reito, S.; Riggi, F.; Romeo, G. Proof-of-Principle of a Cherenkov-Tag Detector Prototype. *Sensors* **2020**, *20*, 3437. [CrossRef]

68. Riggi, F.; Bonanno, D.L.; Bongiovanni, D.; Gallo, G.; La Rocca, P.; Leonora, E.; Longhitano, F.; Lo Presti, D.; Randazzo, N.; Parasole, O.; et al. The Muon Portal Project: Commissioning of the full detector and first results. *Nucl. Instrum. Methods Phys. Res. Sect. A* **2018**, *912*, 16–19. [CrossRef]

69. Lee, S.J.; Chen, Y.; Lodder, B.; Sabatini, B.L. Monitoring Behaviorally Induced Biochemical Changes Using Fluorescence Lifetime Photometry. *Front. Neurosci.* **2019**, *13*, 766. [CrossRef]

70. De Angelis, N.; Heller, M.; Montaruli, T. *Studies of Readout Electronics and Optical Elements for a Gamma-Ray Telescope*; Technical Report; Université de Genève: Genève, Switzerland, 2018.

71. Guberman, D.; Paoletti, R. Silicon photomultipliers in Very High Energy gamma-ray astrophysics. *J. Instrum.* **2020**, *15*. [CrossRef]

72. Gomez, S.; Sanchez, D.; Gascon, D.; Cela, J.M.; Freixas, L.; Graciani, R.; Manera, R.; Marin, J.; Mauricio, J.; Navarrete, J.J.; et al. A High Dynamic Range ASIC for Time of Flight PET with pixelated and monolithic crystals. In Proceedings of the 2019 IEEE Nuclear Science Symposium and Medical Imaging Conference, NSS/MIC 2019, Manchester, UK, 26 October–2 November 2019. [CrossRef]

73. Gómez, S.; Sanmukh, A.; Gascón, D.; Sánchez, D.; Mauricio, J.; Graciani, R.; Manera, R.; Garrido, L.; Fernández-Varea, J.M.; Cela, J.M.; et al. A High Dynamic Range ASIC for Time of Flight PET with monolithic crystals. *Proc. Sci.* **2018**, *343*, 17–21. [CrossRef]